Applied Catalysis B: Environmental 196 (2016) 223–231

Contents lists available at ScienceDirect

Applied Catalysis B: Environmental

journal homepage: www.elsevier.com/locate/apcatb

Noncrystalline nickel phosphide decorated poly(vinyl alcohol-*co*-ethylene) nanofibrous membrane for catalytic hydrogenation of *p*-nitrophenol

Ke Liu[1], Yuan Wang[1], Pan Chen, Weibing Zhong, Qiongzhen Liu, Mufang Li, Yuedan Wang, Wenwen Wang, Zhentan Lu, Dong Wang*

College of Materials Science and Engineering, Wuhan Textile University, Wuhan 430200, China

ARTICLE INFO

Article history:
Received 20 February 2016
Received in revised form 27 April 2016
Accepted 24 May 2016
Available online 25 May 2016

Keywords:
Nanofibrous membrane
Nickel phosphide
Catalyst
Hydrogenation
p-Nitrophenol

ABSTRACT

In this work, we prepare a poly(vinyl alcohol-*co*-ethylene) (PVA-*co*-PE) nanofibrous membrane supported Ni-P nanocatalyst via a melt-phase-separated nanofiber-suspension coating followed by nickel electroless deposition with sodium hypophosphite as the reducing agent. The morphology and structure analysis show that the PVA-*co*-PE nanofibrous membranes (NFM) are decorated by the coating of nickel based nanoparticles on the surface of nanofibers, which is a mixture of Ni and Ni_3P with about 30 nm average nanoparticle size. The 3D nanofibers' scaffold with 4.55 g/m^2 nanofiber coverage density (pore size: 180 nm) affords a best deposited substrate for Ni-P nanoparticles to hydrogenate *p*-nitrophenols (PNP). The supported catalysts exhibit high catalytic rate constant 18.04×10^{-3} s^{-1}, 26.84×10^{-3} s^{-1} and 19.40×10^{-3} s^{-1} at 20 °C when Ni-P loading content is 50 wt.%, 25 wt.% and 14 wt.%, respectively. Furthermore, the catalytic materials present an excellent recoverable and cyclic feature that still over 98% conversion of PNP after 6 times. The outstanding performance obtained here can be attributed to phosphorous doped nanostructure of nickel catalyst, 3D microstructure of nanofibrous membrane and the synergistic effect of nano Ni-P and membrane, including high specific area for holding Ni-P atoms, plenty of electron holes for adsorbing organic molecules, and good conductivity for electron transfer between each decorated nanofibers. Moreover, present Ni-P-based catalyst is relatively cheap, stable and direct separable, implying its superiority in hydrogenation of nitrophenols to aminophenols.

1. Introduction

The *p*-nitrophenol (PNP) is one of the toxic compound extensively used as intermediates in chemical industry [1,2]. Upon use, it is inevitably released into the environmental water bodies due to the insufficient treatment and becomes to a sort of refractory pollutants [3]. On the other hand, *p*-aminophenol (PAP) is an important intermediate in modern fine and pharmacy industry for preparation of several analgesic and antipyretic drugs [4–6]. Based on the application, the world PAP consumption is huge and increases at a rate of 5% per year [7]. Therefore, it is significant important to convert *p*-nitrophenol to *p*-aminophenol by employing the catalyst of large-scale with excellent catalytic performance.

In this reduction reaction, the frequently used catalysts are mainly the noble metal-based materials [8]. However, due to the high cost and scarcity of the noble metal, it is highly desirable to explore alternative catalysts for such reduction [9]. Alternatively, the direct hydrogenation of *p*-nitrophenol catalyzed by transition metal is considered as an alternative green process for the production of *p*-aminophenol [10,11]. Recently, a variety of transition metal phosphide nanomaterials has been investigated and characterized as potential hydrogenation reaction catalysts due to their higher catalytic activity and much better stability than pure metal and other interstitial compounds [12,13]. Among these, nickel phosphides have attracted great attention for hydro-deoxygenation [14,15], hydrogenations of CO [16], Hydroisomerization of *n*-dodecane [17] and acetonitrile [18]. However, this type of catalyst has rarely been reported to be utilized on the hydrogenation of PNP hitherto.

Normally, the metal catalysts are synthesized in the form of micro- or nano-particles due to the rapid preparation process. However, direct application of metal nanoparticles in water treatment encounters enormous challenges against the rapid agglomeration and perpetual suspension, which dramatically lowers their

* Corresponding author.
E-mail address: wangdon08@126.com (D. Wang).
[1] These authors contributed equally to this work.

http://dx.doi.org/10.1016/j.apcatb.2016.05.059
0926-3373/

catalytic activities [19]. A constructive approach is integrating metal particles into unique 3D nanofibrous structure [20], endowing the metal nanoparticles with improved catalytic property and recyclability [21]. On account of this effect, various macroscopic materials have been proposed to support nanoparticles. Examples include colloidal particles [22–24], nanostructured thin films [25], polymeric hollow fiber membranes [26], anodic aluminum oxide (AAO) membranes [27], photolithographic Si microwire arrays [28], foam Ni scaffolds [29,30] and so on. Compared to these, the immobilization of metal nanoparticles on nanofibers via chemical modification for producing functional nanocomposites recently has been more attractive such as carbonaceous nanofibers membrane [20] and cellulose nanofibres of filter paper [21]. Such 3D nanomaterials possess significant advantages of highly specific surface area, high functionalized surfaces, and easy handling for assembling catalytic matters [20]. Although the structures and properties of 3D nano-materials are distinctively different from those of bulk materials, nickel phosphides with interconnected 3D nano-networks have never been synthesized till now. Therefore, it is extremely valuable to enhance rather than compromise the properties of nanoscale nickel phosphide through supporting them by special nano-materials with unique 3D structure like nanofibrous membrane.

PVA-*co*-PE is a common polymer with abundant hydroxylic groups, facilitates the modification of them with given chemicals or nanoparticles. In our previous works, PVA-*co*-PE nanofiber membranes have been handled and successfully applied in fields as diverse as filtration [31], adsorption [32], antibacterial [33], biosensor [34] and food sensor [35]. In this contribution, we fabricated PVA-*co*-PE nanofiber membranes with 3D nanostructure via melt phase separation and suspension coating technique. Sequently, Ni-P decorated nanofibrous membrane was prepared by electroless depositing nickel with sodium hypophosphite as the reducing agent. Furthermore, the feasibility of as-prepared nanocomposite was demonstrated in the catalytic reduction of *p*-nitrophenol (PNP). The recycle tests were also performed to assess the comprehensive catalytic property.

2. Experimental

2.1. Materials

PVA-*co*-PE (44% ethylene unit) was purchased from Sigma-Aldrich (Milwaukee, WI, USA). CAB (butyryl content 35–39%) was purchased from Acros Chemical Pittsburg, PA, USA). stannous chloride hydrate ($SnCl_2{\cdot}2H_2O$), palladium Chloride ($PbCl_2$), nickle sulfate hexahydrate ($NiSO_4{\cdot}6H_2O$), sodium hypophosphite monohydrate ($NaH_2PO_2{\cdot}H_2O$), Sodium borohydride ($NaBH_4$, 96%), lactic acid, trisodium citrate dihydrate ($Na_3C_6H_5O_7{\cdot}2H_2O$), sodium acetate anhydrous, isopropyl alcohol, acetone, concentrated hydrochloric acid, 4-nitropheno were all analytical reagent grade. Triton X-100 was chemical reagent grade. They were all obtained from Sinopharm Chemical Reagent Co., LTD. All chemicals used in the experiments were used without further purification.

2.2. Preparation of nanofibrous membrane

PVA-*co*-PE nanofibers were prepared according to methods reported in our previous work [36]. The mixed PVA-co-PE and CAB pellets (w/w = 20/80) was fed into a Leistritz corotating twin-screw (18 mm) extruder (Model MIC 18/GL 30D, Nurnberg, Germany) at a feed rate of 12 g/min. Twin-screw extruder processing temperature parameters ranged from 190 to 230 °C. The blends were extruded with a draw ratio of 25 (the area of cross section of the die to that of the extrudates) and cooled by water. PVA-*co*-PE NFs in form of continuous yarns were prepared by the Soxhlet extraction of CAB matrix via acetone. After being dried, the nanofibers were dispersed in an aqueous solution with a high speed shear mixer to form a stable suspension. The suspension was then coated on a soft polyethylene (PE) film substrate with nanofiber coverage densities (3.81, 4.55, 5.04, 6.48 and 7.16 g/m^2) by spraying method. The nanofiber layer was dried until constant weight and subsequently removed from the substrate.

2.3. Preparation of Ni-P decorated PVA-co-PE nanofibrous membrane (Ni-P/NFM)

As shown in Scheme 1, the nanofibrous membranes were cut into pieces with weight of 3 mg and treated with a surface sensitizer consisting of a mixture of 10 g L^{-1} $SnCl_2$ and 30 mL L^{-1} HCl by slow agitation at 30 °C for 3 min. The sensitized fabrics were subsequently rinsed with deionized water. The samples were then immersed in an activator composed of 0.25 g L^{-1} $PdCl_2$ and 20 mL L^{-1} HCl at 25 °C for 5 min. The fabrics were then immersed in a 200 mL Ni plating solution containing $NiSO_4{\cdot}6H_2O$ (0.77 mol L^{-1}), $NaH_2PO_2{\cdot}2H_2O$ (22 g L^{-1}), CH_3COONa (30 g L^{-1}), Triton X-100 (5 mg L^{-1}) and $Na_3C_6H_5O_7{\cdot}2H_2O$ (10 g L^{-1}) at 40 °C for 2 min. The plating solution was adjusted to a pH of 5.0 by using lactic acid. After the electroless deposition, Ni-P/NFMs with varied nanofiber coverage density (3.81 g m^{-2}, 4.55 g m^{-2}, 5.04 g m^{-2}, 6.48 g m^{-2}, 7.16 g m^{-2}) were rinsed with deionized water and then dried in an oven at 50 °C. The physical parameters of membranes before and after deposition are shown in Table 1. With the same depositing condition, the Ni-P decorated PVA-*co*-PE plate membrane (Ni-P/PM) was prepared by immersing the spin coated PVA-*co*-PE plate membrane into the nickel plating solution.

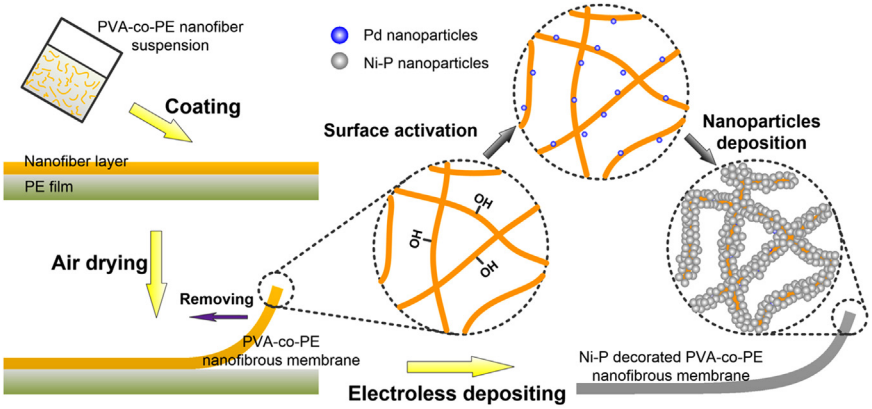

Scheme 1. Schematic image of preparation process of Ni-P/NFM.

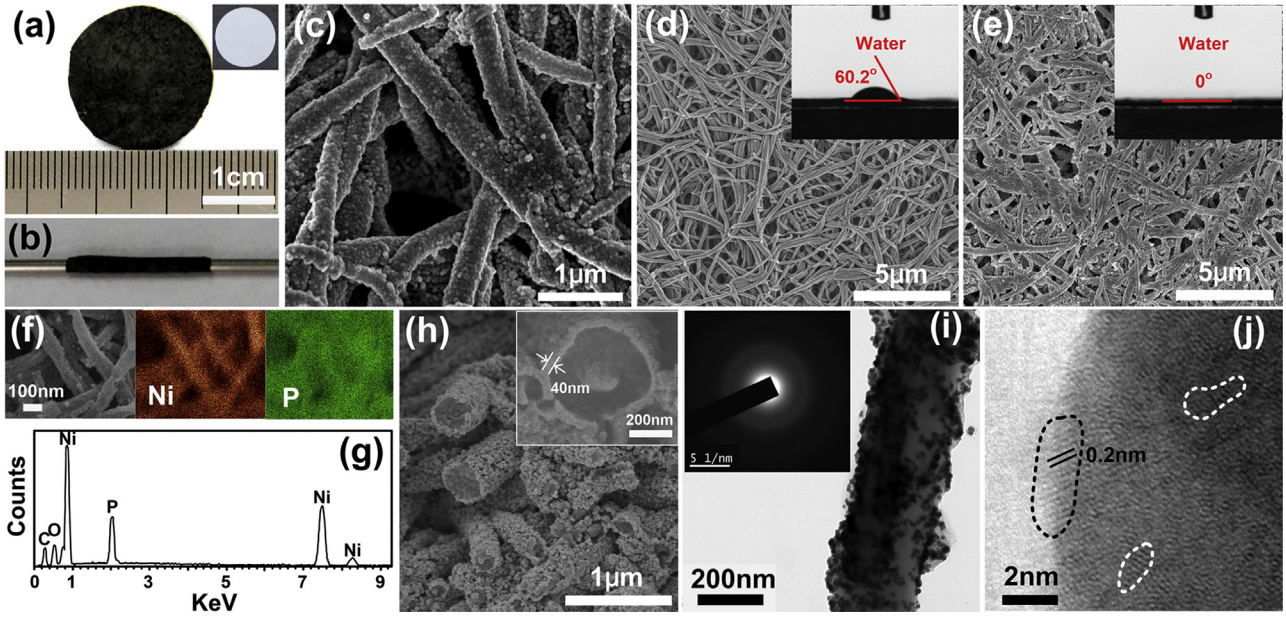

Fig 1. Ni-P decorated PVA-*co*-PE nanofibrous membrane with nanofiber coverage density 4.55 g/m^2 (Ni-P/NFM$_{4.55}$). (a) Digital photos of Ni-P/NFM$_{4.55}$ and the relative pristine PVA-*co*-PE nanofibrous membrane (NFM) in insert image. (b) Rolled Ni-P/NFM$_{4.55}$ around the steel rod. SEM images of (c) Ni-P/NFM$_{4.55}$ surface and (h) its cross section. SEM images and contact angle of (d) PVA-*co*-PE NFM and (e) Ni-P/NFM$_{4.55}$. (f) The elemental distribution mapping and (g) EDS spectrum of Ni-P/NFM$_{4.55}$. (i) TEM of single nanofiber decorated by Ni-P nanoparticles, the insert of (i) is the corresponding SAED pattern, (j) The HRTEM image of Ni-P nanoparticle.

2.4. Characterization

The scanning electron microscopy (SEM) images, energy-dispersive X-ray spectroscopic analysis (EDS), and emission scanning electron microscope elemental distribution mapping of specimens were taken by a JEOL JSM-6510 L scanning electron microscope equipped with energy-dispersion X-ray fluorescence analyzer. Prior to examination, the specimens were sputtering coated with gold.

The distribution of Ni-P nanoparticles on the nanofibers were evaluated by using a JEOL JEM-2010FEF transmission electron microscope (TEM). Before the test, the nanofibers were ultrasonically suspended from small membrane fragment in ethanol for 1 h and collected by copper grid.

The crystal structures of Ni-P/NFMs were characterized by using a wide angle X-ray diffractometer (X'PertPRO, PANalytical, Almelo, Netherlands) operating at 45 kV and 44 mA. The wide angle X-ray diffraction patterns were recorded from 10° to 80° with a step width of 0.0170° and a scanning rate of 5°/min. To improve the crystallization, the membrane was calcinated at 773 K for 2 h in argon atmosphere. The X-ray photoelectron spectra (XPS) measurement was performed on a VG MultiLab 2000 X-ray photoelectron spectrometer (Thermo Electron Corporation) using Mg-Kα ($h\nu$ = 1253.6 eV) radiation as the excitation source.

The pore sizes and distributions of nanofiber membranes were examined using a capillary flow porometer (Model CFP-1500A, PMI Inc., USA). The contact angle goniometry (KRUSS DSA30S, KRUSS Co., Germany) was used to evaluate hydrophilicity of membranes and at least five different places on each sample were tested for consistency.

2.5. Catalytic property

Catalytic activity in the reduction of *p*-nitrophenol to *p*-aminophenol by excess $NaBH_4$ was used as a model reaction to evaluate the catalytic activity of Ni-P/NFMs with different area (shown in Table 1) and same Ni-P nanoparticles weight (3 mg). Furthermore, to compare the catalytic activities of Ni-P/NFMs with referenced catalytic specimens, the catalytic activity of Ni-P/PM and commercial RANEY Ni were also investigated. The catalytic redox reaction process was set up in a standard quartz cuvette with 1 cm path length and 3 mL volume as a small batch reactor. In the first step, Ni-P/NFMs (or Ni-P/PM) with 3 mg Ni-P (or 3 mg RANEY Ni) was introduced to the above quartz cuvette containing *p*-nitrophenol (3 mL, 0.5 mM) at 20 °C and kept for 20 min without stirring. Next, 0.3 mL of freshly prepared aqueous solution of $NaBH_4$ (1.0 M) were added to the above solution and time-dependent absorption spectra were measured. This reaction was monitored by a Shimadzu UV2700 spectrophotometer over a scanning range of 200–500 nm at 20 °C. The rate constant of the reaction was measured by the extinction of the solution at 400 nm (absorption of *p*-nitrophenolate ion) as a function of time.

Table 1
Physical parameters of membranes before and after deposition.

Specimen	Membrane before deposition			Membrane after deposition	
	Mass/mg	Area/cm^2	Thickness/μm	Mass/mg	Area[a]/cm^2
Ni-P/NFM$_{7.16}$	3.05	4.26	13.43	7.00	3.24
Ni-P/NFM$_{6.48}$	2.97	4.58	12.22	6.59	3.51
Ni-P/NFM$_{5.04}$	3.03	5.58	11.47	6.38	4.43
Ni-P/NFM$_{4.55}$	2.88	6.33	9.07	5.86	6.37
Ni-P/NFM$_{3.81}$	3.16	8.64	7.04	9.76	4.00

[a] This is the area of Ni-P/NFMs containing 3 mg Ni-P nanoparticles for catalysis test.

3. Results and discussion

3.1. Morphology and structure

As shown in Fig. 1a, the as-prepared Ni-P/NFM$_{4.55}$ presents black gray color compared to the white polymeric nanofiber membrane (see inserted image in Fig. 2a), suggesting that the surface of PVA-*co*-PE nanofibers were converted into metal phosphides. The rolled Ni-P/NFM$_{4.55}$ around the steel rod indicates the flexibility of the composite membrane (Fig. 1b). Upon closer observation of high-magnification SEM image, it was found that the nanofibers are

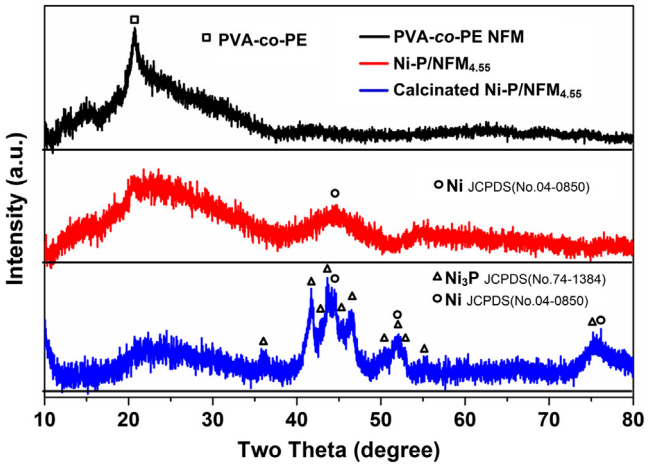

Fig. 2. XRD patterns of PVA-*co*-PE nanofibrous membrane, Ni-P/NFM$_{4.55}$ and calcinated Ni-P/NFM$_{4.55}$ (For interpretation of the references to color in the text, the reader is referred to the web version of this article.).

uniformly covered by numerous nanoparticles with a size from about 10 nm to 70 nm (Fig. 5e). From the view of cross section image of Ni-P/NFM$_{4.55}$ in Fig. 1h, it is obvious that the nanoparticles are densely deposited on PVA-*co*-PE nanofibers and shows a core-shell structural profile with about 40 nm shell thickness, which reduces the pore size of membrane consistent with the morphology of membranes shown in Fig. 1d and e. Moreover, the metal-rich surface also results in a distinct change on the hydrophilicity with the water contact angle of membranes decreasing from about 60.2° to 0° (inserted ones in Fig. 1d and e) implying its priority in aqueous-phase catalysis. EDS point-scan spectrum and EDS elemental mapping indicate that Ni and P are the main elemental components uniformly distributed on the surface of whole PVA-*co*-PE nanofibrous skeleton, of which the main elements C and O is detected as shown in Fig. 1g.

To further investigate the microstructure of the nanoparticles growing on the nanofibrous membrane, the as-obtained Ni-P/NFMs was sonicated continuously for 1 h to exfoliate nanofibers from the membrane. TEM images in Fig. 1i also verify their core-shell morphology. For exfoliated nanofibers, the halo ring rather than distinct dots shown in selected area electron diffraction (SAED) (inset of Fig. 1i) suggests the noncrystalline structure of the as-prepared Ni-P particles. The detailed structures of exfoliated Ni-P nanoparticles were revealed by high-resolution transmission electron microscopy (HRTEM). Fig. 1j shows a typical HRTEM image of Ni-P nanoparticles exfoliated from specimen Ni-P/NFM$_{4.55}$. The structure is basically disordered. However, there are some partially ordered nanodomains as confirmed by the short-range lattice fringes, with the dimension as small as 1 nm indicated by white dot lines. The d-spacing of these fringes in the domains is about 0.20 nm, which correlates well with the (111) spacing of Ni [37]. The corresponded X-ray diffraction peak locates at 2θ of ~44.6° as depicted in red line of Fig. 3. In addition, the peak at 2θ of 21.7° shown in this spectrum belongs to the XRD pattern of PVA-*co*-PE nanofibrous membrane (NFM) as distinctly indicated in black line.

For better verifying the structure and composition of Ni-P/NFMs, Ni-P/NFM$_{4.55}$ was calcined at 773 K for 2 h in argon atmosphere. It was found that the calcinated sample possesses the crystalline feature of Ni_3P and Ni proved by XRD (blue line in Fig. 2). This result suggests that the actual Ni/P atom ratio is larger than 3:1, which is in concordance with the results evaluated from XPS spectrum 3.74:1 (Fig. 3) and the knowledge that the nickel-containing electroless coating is a mixture of Ni and Ni_3P [38]. Additionally, it is reported that Ni_3P shows higher catalytic activity than other nickel-rich phosphide catalysts such as Ni_2P and $Ni_{12}P_5$ because the high ratio of nickel to phosphorus provides more chance for the exposure of metal nickel to the reactants [12].

Fig. 3 shows XPS spectra of Ni and P elements for Ni-P/NFM$_{4.55}$. The Ni $2p_{3/2}$ spectrum consists of several components, in which the peaks around 852.1, 855.4 and 860.8 eV attribute to $Ni^{\delta+}$ in Ni-P, oxidized Ni species and the satellite of Ni $2p_{3/2}$ peak, respectively. For the Ni $2p_{1/2}$ energy level, three peaks at 869.3, 873.0 and 878.7 eV are assigned to $Ni^{\delta+}$ in Ni-P, oxidized Ni species and the satellite of the Ni $2p_{1/2}$ peak, respectively [13,39]. Additionally, In Fig. 3b, peaks at 129.5 eV and 132.5 eV can be assigned to $P^{\delta-}$ in Ni_3P and oxidized P species [13,39], respectively. It can be concluded that $Ni^{\delta+}$ and $P^{\delta-}$ indicate the electron transfer from Ni to P in all Nickel phosphide [39,40]. The oxidized Ni and P species in specimen are contributed to the passivation of the catalysts when exposed to air [41].

3.2. *Catalytic performance for hydrogenation of* p-*nitrophenols*

The reduction of PNP by $NaBH_4$ in the presence of nickel-based catalyst is a well-studied green chemical reaction [10]. As known to all, the catalytic performance is dependent on the morphology and distribution of nano-catalyst materials. For this aim, the effect of substrate and Ni-P loading content on the catalysis activity to the reduction of PNP was investigated. In our experimental, the yellow color of solution gradually fades with time assisted by catalyst, and detected by measuring the disappearance of UV-spectrum peak at 400 nm corresponding to the *p*-nitrophenolate ion in the presence of $NaBH_4$ [42]. Fig. 4a shows that the degradation of peak at 400 nm is accompanied by the emerging peak at 315 nm suggesting that PNP was reduced to *p*-aminophenol with the introduction

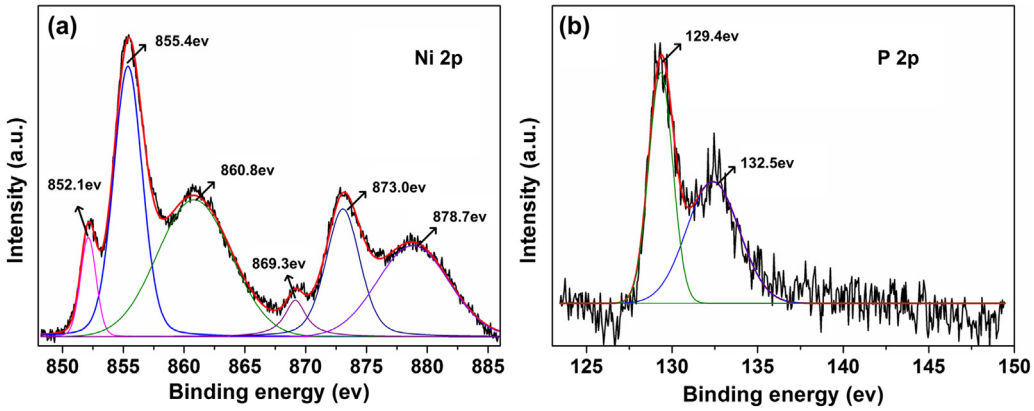

Fig. 3. XPS spectra of (a) the Ni 2p and (b) the P 2p regions for Ni-P/NFM$_{4.55}$.

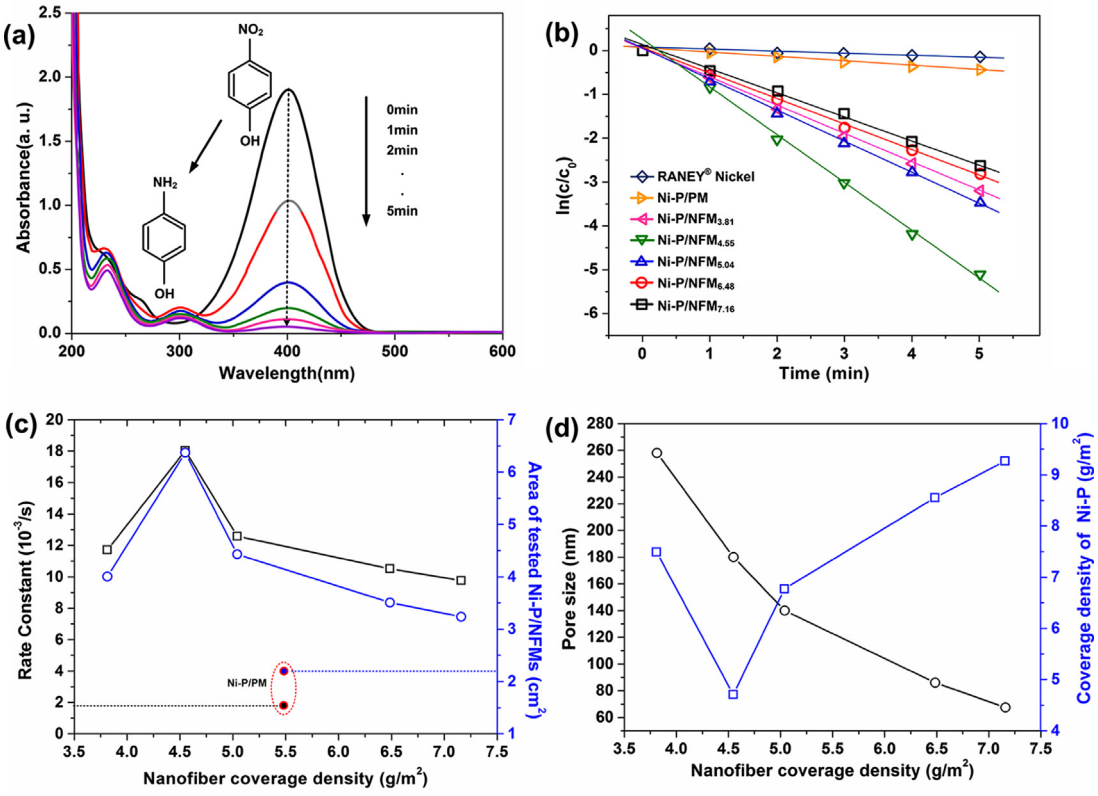

Fig. 4. (a) UV–vis absorption spectra of PNP reduced to PAP by $NaBH_4$ in the present of Ni-P/$NFM_{4.55}$ at a certain time interval, (b) Pseudo-first-order plot of $\ln(c/c_0)$ against reaction time for the hydrogenation of PNP over different catalysts with different nanofiber coverage density, (c)Varied rate constant, area of tested Ni-P/NFMs depended on nanofiber coverage density, (d) Relationships between NFM pore size, Ni-P coverage density and nanofiber coverage density (NFCD).

of Ni-P/$NFM_{4.55}$. In the test, $NaBH_4$ provided is much more than PNP (~200:1) so that the kinetics of this reaction can be treated as a pseudo-first-order reaction [2]. The catalytic ability can be estimated by rate constants k calculated by equation:

$$k = \frac{\ln\left(c/c_0\right)}{t} = \frac{\ln A}{t} \quad (1)$$

where A is the absorbance at 400 nm, c_0 is the initial concentration of PNP, t is reaction time in second. c is the concentration of PNP after reacting for t.

3.2.1. *Effect of nanofiber coverage density on the catalytic performance*

The pseudo-first-order plots of $\ln(c/c_0)$ against reaction time for hydrogenation of PNP over specimens were displayed in Fig. 4b. Due to the induction time, it is reasonable to estimate the rate constant without regard to the data at 0 s [43]. It is obvious that membrane-supported Ni-P nano-materials showed higher catalytic activity than the commercial porous materials RANEY® Ni. This is partly derived from the addition of phosphide into the active catalyst Ni [44]. On the other hand, the nanofibrous membrane materials play as a great dispersion substrate. Additionally, Ni-P/NFMs present higher catalytic performance than Ni-P/PM implying that the nanofibrous membrane provides a better support for dispersing the catalysis materials and enhancing the actual catalytic activity. From Fig. 7a and b, one can see that Ni-P/NFM possesses much more interconnected pores on the surface of membrane compared with Ni-P/PM due to the nature of nanofiber nonwoven, which presents higher porosity and larger specific area [45]. As a result, a large amount of Ni-P nanoparticles distribute in nanofibrous membrane per unit area providing more active sites for enhancing the reaction speed.

Furthermore, with the nanofiber coverage density (NFCD) increasing, the rate constant of Ni-P/NFMs exhibits a trend of rise first and decrease afterwards with an inflection point at NFCD = 4.55 g/m^2 (Fig. 4c). It has been reported that the catalytic activity is in correlation with nanoparticle size and the distribution determined by the substrate for the same chemical component [2,44]. In this work, Ni-P nanoparticles in Ni-P/$NFM_{3.81}$, Ni-P/$NFM_{4.55}$ and Ni-P/$NFM_{7.16}$ show the similar size distribution to each other with the average size of 28.8 nm, 28.4 nm, 34.3 nm, respectively, as shown in Fig. 5e–g. Herein, it can be concluded that the catalytic activity of Ni-P/NFMs varied with NFCD is mainly attributed to the 3D structure of PVA-*co*-PE nanofibrous membranes rather than nanoparticle size. To eliminate the effect of Ni-P loading on the catalytic activity, the membrane specimens were tailored to keep the weight of Ni-P nanoparticle at 3 mg for each sample. Either rate constant or area of Ni-P/NFMs are both larger than that of Ni-P/PM suggesting that Ni-P nanoparticles are better dispersed and the catalytic performance are better enhanced based on nanofibrous membrane (Fig. 4c). The actual area of nanofibrous mambrane is shown in Table 1 and Fig. 4c, from which it can be seen that the area presents a same trend with that of rate constant varied by nanofiber coverage density. It indicates that the rate constant of Ni-P/NFMs has the internal relation with the area of membrane. This is because that more catalytic active sites provided by bare Ni-P nanoparticles can be realized by nanofibrous membrane with larger area.

Ni-P/NFMs area altering with NFCD can be explained as follows. Fig. 4d illustrates that the membrane with higher NFCD has the pore with smaller size due to the layer-by-layered nanofiber stacking, which is an essential feature of nanofiber-based membrane [46]. With the pore size decreases, the number of nanofibers stacked on the surface of membrane per unit area increase. It results in

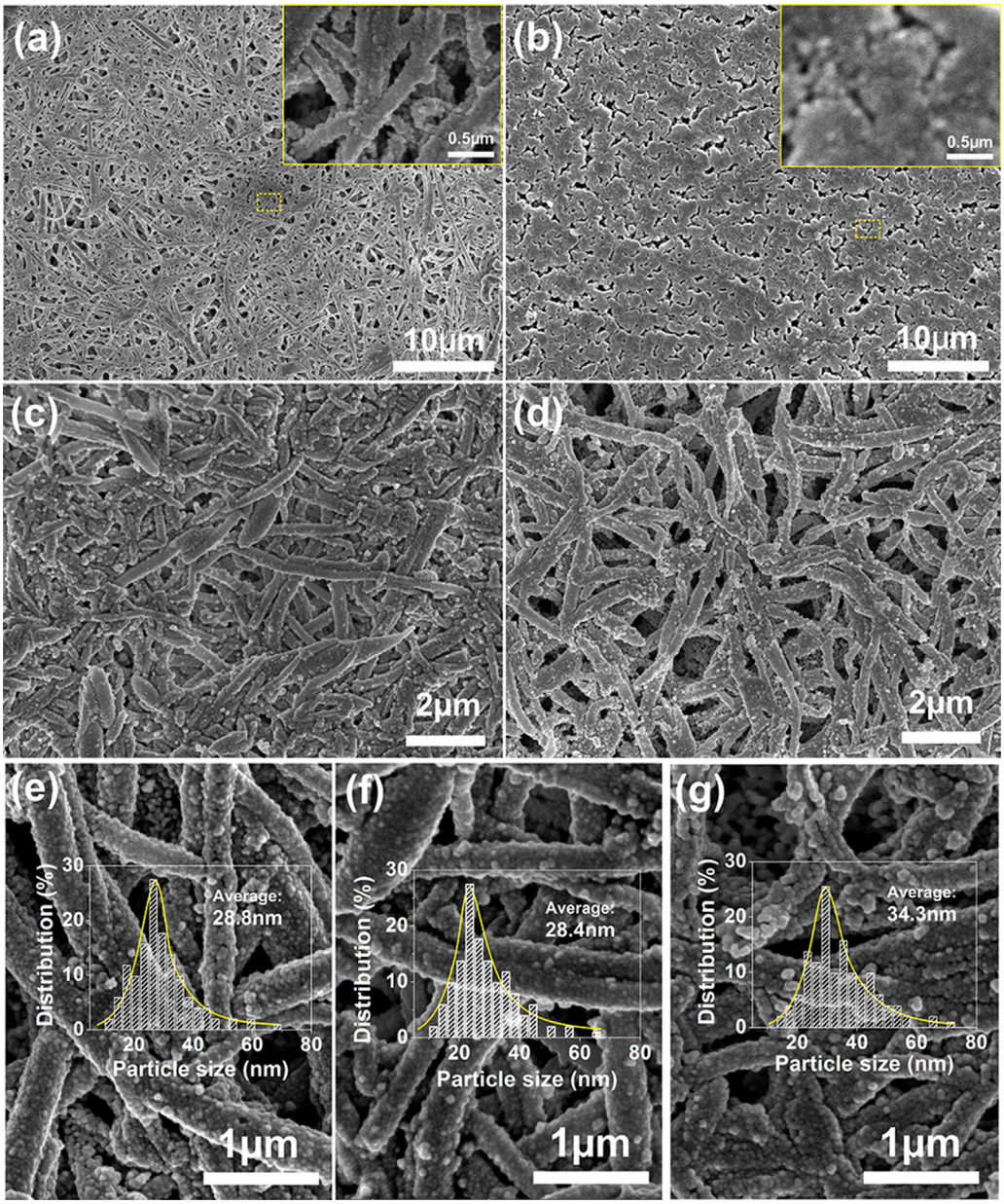

Fig. 5. SEM image of (a) Ni-P/NFM$_{4.55}$, (b) Ni-P/PM, (c) Ni-P/NFM$_{3.81}$ and (d) Ni-P/NFM$_{7.16}$, morphology and Ni-P nanoparticle size distribution of (e) Ni-P/NFM$_{3.81}$, (f) Ni-P/NFM$_{4.55}$ and (g) Ni-P/NFM$_{7.16}$.

more sites for depositing and the loading content of Ni-P nanoparticles increasing in the surface region as shown in Fig. 5c and d. As a result, the membrane with small pore size can consume more nickel bath ions and create high concentration gradient, which further enhances the diffusive capability of nickel bath ions to membrane surface. This is also the main reason why the nanoparticle size on Ni-P/NFM$_{7.16}$ is larger than other membranes as shown in Fig. 5g. On the other hand, smaller pore size can influence the mass transfer of bath ion from the surface to the interior of membrane [47] leading to lower the number of Ni-P nanoparticles deposited on the surface of nanofibers inside of membrane in each unit area as shown in Fig. 6b.

For nanofibrous membrane, the weight of Ni-P nanoparticles consists of two parts in unit area of membrane. One is derived from the deposition in the surface region m_s, and another comes from the plating in the interior region m_i. Therefore, it is highly possible that the total weight $m = m_s + m_i$ of Ni-P nanoparticles in unit area of membrane, i. e. CD of Ni-P, increase first and then decrease with the pore size increase. Although it is difficult to decide the numerical curve shape of *m_s-pore size* and *m_i-pore size* as well as the value of pore size at the smallest CD of Ni-P (see dot lines in Fig. 6a), it provides a reasonable explanation to the relationship between CD of Ni-P and NFCD (Fig. 4d) and that between the area of tested Ni-P/NFMs and NFCD (Fig. 4c).

Therefore, designing 3D structure of nanofibrous membrane is an effective approach to disperse catalyst nanoparticles adequately. In this work, the optimum NFCD for loading NI-P nanoparticles is 4.55 g/m^2. Besides, for this case, a larger membrane area also help to grow finer nanoparticle through reducing the concentration gradient of nickel bath ion near the surface of nanofibers in agreement with the previous report [48].

3.2.2. *Effect of Ni-P loading on the catalytic performance*

Based on previous results, nanofibrous membrane with 4.55 g/m^2 NFCD was chosen as the substrate to support Ni-P with different loading content, which was achieved through changing

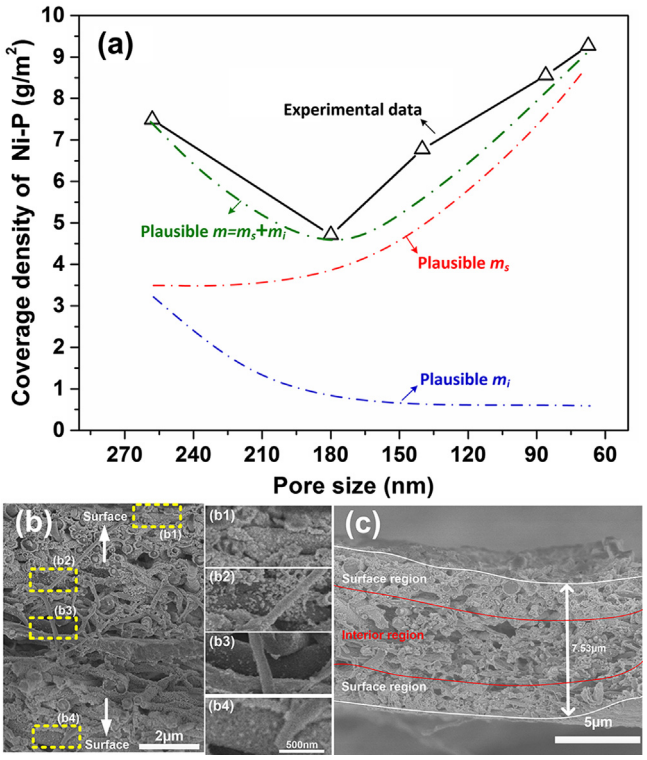

Fig. 6. (a) Relationship between coverage density (CD) of Ni-P and CD of Ni-P, (b) SEM of cross section of Ni-P/NFM$_{4.55}$ with (b1), (b2), (b3) and (b4) the enlarged image of regions with different distance to the surface, (c) the schematic surface and interior regions indicated on the cross section of Ni-P/NFM$_{4.55}$.

the electoless deposition time. Fig. 7 shows that the rate constant almost keeps constant with Ni-P content increasing from 50 wt.% (3 mg on 3 mg NFM) to 63 wt.% (5 mg on 3 mg NFM). When the weight percentage of deposited Ni-P decreases to 25% (1 mg on 3 mg NFM), k presents a maximum value of 26.84 s^{-1}. Ni-P/NFM$_{4.55}$ with lower (smaller than 25 wt.%) or higher (larger than 25 wt.%) Ni-P content results in relative lower rate constant compared to Ni-P$_{0.25}$/NFM$_{4.55}$. The former one is mainly originated from low Ni-P content correlation with a smaller amount of active site. While the major cause of the later one probably is that longer deposition time tend to generate a smaller membrane pore size and larger Ni-P particle size.

Additionally, it should also be noted that rate constant k in Eq. (1) is an apparent one depending on the usage of PNP and catalysts. For a better understanding, the kinetic parameter turnover frequency (TOF) is employed to estimate the catalytic activity of Ni-P/NFM$_{4.55}$ [49]. Fig. 7 exhibits that with the loading content of Ni-P increases, TOF of Ni-P/NFM$_{4.55}$ continue to decrease suggesting the actual usage of Ni-P nanoparticles contributes a lot for this parameter. However, it has been found that a very few loading content of Ni-P (e.g. ≤14 wt.%) will leads to the exposure of PVA-*co*-PE nanofiber in the air further impact the service life of membrane supported catalyst (not shown in this work). Herein, catalyst with high Ni-P content (such as Ni-P$_{0.25}$/NFM$_{4.55}$ and Ni-P$_{0.5}$/NFM$_{4.55}$) is suitable for application in practice.

In Table 2, we compared the catalytic capacities of Ni-P/NFMs in this work with the data in other literatures. From Table 2, it is distinct that the Ni-P$_x$/NFM$_{4.55}$ (x = 0.14, 0.25, 0.50) in present work is some of the best catalysts reported for the hydrogenation of PNP even compared to the noble metallic catalyst CNTM supporting Au [2,9,13,19,50–54]. Although the rate constant is smaller than that of Ni-B nanotube [51], the flexibility of Ni-P/NFM$_{4.55}$ endows our materials more convenience for actual application. TOF of Ni-P$_{0.25}$/NFM$_{4.55}$ lower than some referenced data indicates that it is necessary to study the better condition of preparation and application of Ni-P$_{0.25}$/NFM$_{4.55}$ in the future. It is believed that the factors including longer absorption time of PNP, lower usage of PNP, stirring, smaller nanofiber diameter and smaller Ni-P nanoparticle size via adjusting nickel bath condition are all of highly possibility to further improve the catalytic activity of Ni-P/NFMs.

3.2.3. *Cycling performance*

To explore hydrogenation catalysts with comprehensive performance, it is of great importance to investigate the recoverability and reusability. The Ni-P/NFM$_{455}$ catalysts were used in the reduction reaction of PNP for 5 min at 20 °C over 6 cycles. After each catalytic reaction, the membrane catalysts were reused after being directly put out of reaction solution, washed with absolute ethyl alcohol and dried in the air at 60 °C for 30 min. As shown in Fig. 8, after used for 6 successive cycles, the rate constant of Ni-P$_{0.25}$/NFM$_{455}$ and Ni-P$_{0.5}$/NFM$_{455}$ was only slightly decreased as compared to fresh catalysts. The conversion efficiency still maintained over 98%, which is similar to the referenced nickel-based catalyst [53] but with a much easier recovery treatment (without using magnet, used in form of whole membrane). However, after RANEY® Ni was used for only 3 times under the same condition, the rate constant rapidly decreased from 0.36 × 10^{-3}/s by about 84%. Only 3% conversion can be reached, suggesting the convenient recoverability and excellent stability of Ni-P/NFMs for the catalytic reaction.

3.2.4. *Catalytic mechanism for* p*-nitrophenols hydrogenation*

On the basis of the above observations and literatures [4,51,53,55], we propose a plausible mechanism of present reduction process as shown in Scheme 2. Firstly, in the reduction system,

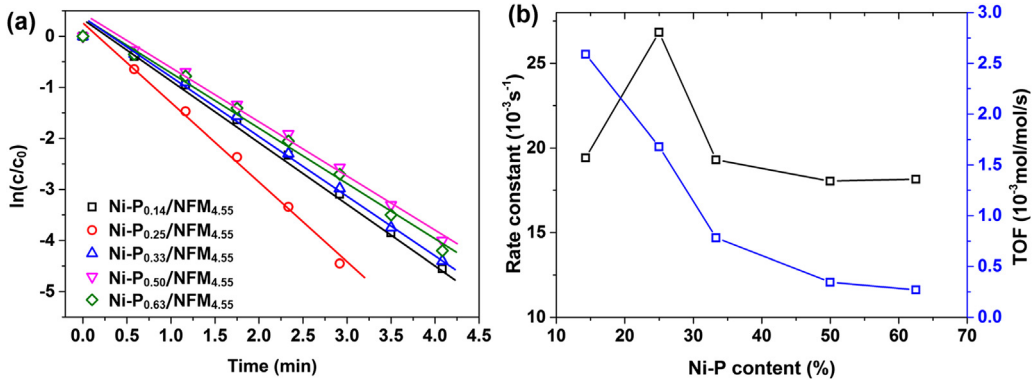

Fig. 7. (a) Pseudo-first-order plot of ln(c/c_0) against reaction time for the hydrogenation of PNP over different catalysts with different Ni-P loading content, (b) Varied rate constant, TOF of tested Ni-P$_x$/NFMs (x = 0.14, 0.25, 0.33, 0.50, 0.63) depended on Ni-P content.

Table 2
Comparison of the catalytic capacities of various catalysts reported in the literature for the reduction of PNP by $NaBH_4$ at room temperature.

Materials	Rate constant (10^{-3}/s)	TOF[a] (10^{-3}mol/mol/s)	Molar ratio ($NaBH_4$: Nitrophenol)	Reference
Ni-$P_{0.14}$/$NFM_{4.55}$	19.40	2.59	200	This work
Ni-$P_{0.25}$/$NFM_{4.55}$	26.80	1.83	200	This work
Ni-$P_{0.50}$/$NFM_{4.55}$	18.04	0.35	200	This work
Ni	2.70	0.006	200	2
Bi_2O_3	1.16	0.14	70	9
CNTM/Au	13.30	2.64	250	19
RGO/Ni	0.24	0.03	300	50
Ni-B nanotube	47.00	2.32	200	51
Ni_xP_y[b]	9.50	0.93	333	52
$Ni_{0.22}$/CB	2.31	2.73	106	53
Pd/PESM	0.30	7.28	20	54

[a] TOF = the mole of PNP per mole of catalyst per second when PNP reached full (100%) conversion.
[b] The temperature has not been introduced in the literature.

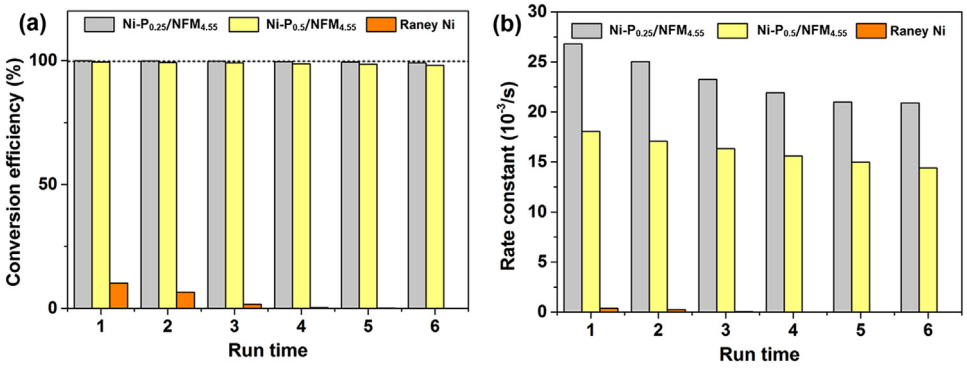

Fig. 8. Cycling performance of Ni-$P_{0.25}$/$NFM_{4.55}$, Ni-$P_{0.5}$/$NFM_{4.55}$ and RANEY® Ni catalysts for PNP reduction.

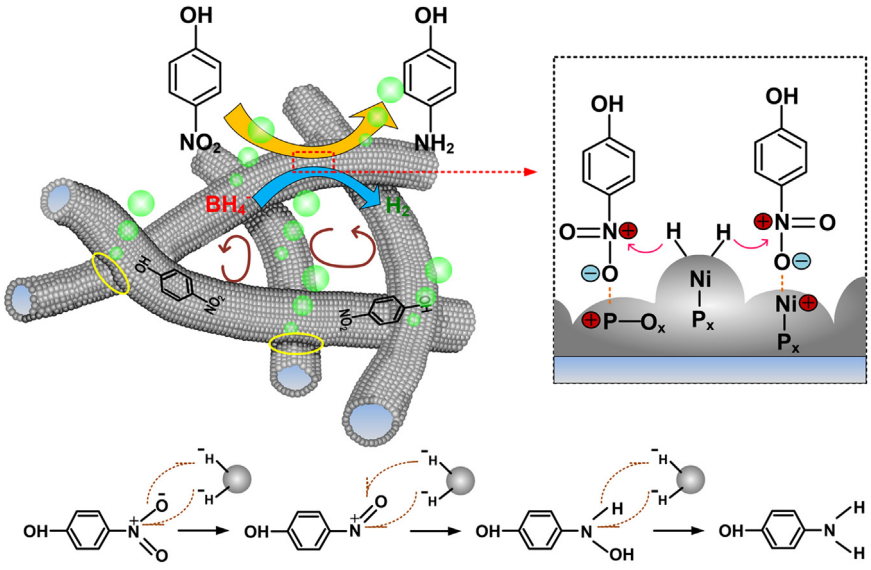

Scheme 2. Proposed plausible mechanism for the reduction of *p*-nitrophenol catalyzed by the Ni-P/NFMs in the presence of $NaBH_4$ (For interpretation of the references to color in the text, the reader is referred to the web version of this article.).

the high specific surface area, $P^{\delta+}$ on the catalyst surface and the $Ni^{\delta+}$ in Ni_3P play an important role in promoting the interaction between Ni-P/NFMs and nitrophenols [4,55]. Secondly, $NaBH_4$ reacts with water at room temperature to slowly produce H_2 and $NaBO_2$. In the presence of Ni-P nanoparticles, H_2 cleaving is activated to generate Ni-H species as a reducing agent [51]. Thirdly, the fixed *p*-nitrophenol on the surface of catalyst can be readily attacked by the hydrogen with a partial negative charge, and then turn to *p*-aminophenol by the reductive addition of two hydrogen atoms [53]. Finally, the generated *p*-nitrophenol is desorbed from the surface of the catalyst.

Therefore, the advantage of observed Ni-P/NFMs lies in following factors:

(1) *Nocrystalline structure*. The as-electroless-deposited Ni-P nanoparticles supported by nanofibrous membrane demonstrate a characteristic structure that is ordered within a short range, but disordered at longer ranges. It facilitates the formation of several surface-inducing unsaturated sites and the lack of crystal defects resulting in an excellent activity of catalyst [51,56].

(2) *Interconnected porous structure*. The nanofibrous membrane were stacked by thousands of nanofibers and present 3D open-cell network that is composed of interconnected holes in nanoscale, and decorated by compact films of Ni-P nanoparticles. The structure exhibits confinement effects on the reactant molecules and increase their collision probability with the open-cell walls [57] (see brown arrows in Scheme 1). This helps to generate more active catalytic sites, higher catalytic activities and catalytic efficiency [58].

(3) *Phosphorous effect*. The introduction of appropriate amount of phosphorous into nickel contributes to the enhancement of the deoxygenation activity of the catalyst surface via $P^{\delta+}$ [55] and the high stability of nickel based catalyst materials [59]. Additionally, phosphorus in Ni_3P draws the electron from nickel, which improves the electrostatic adsorption between $Ni^{\delta+}$ and nitrophenole ion [4,57].

(4) *Nanofibrous network*. Nanofibrous network is beneficial to the formation of networks of compact Ni-P nanofilms. Thereby, the electron can easily transfer along the Ni-P coating from one nanofiber to another through the connections [35] (noted by yellow circle in Scheme 1) and increases the local electron density, facilitating the uptake of electrons by PNP molecules [53].

As a result, the synergistic effect of noncrystalline 3D porous configuration and phosphorus doping finally causes an extremely comprehensive catalytic performance for PNP reduction. This work develops a facile approach to manufacture cheap and efficient nanocatalyst for the treatment of *p*-nitrophenol-like pollutants.

4. Conclusion

In summary, a poly(vinyl alcohol-co-ethylene) (PVA-*co*-PE) nanofibrous membrane supported Ni-P nanocatalyst was successfully prepared via by facile nickel electroless deposition method based on polymeric nanofibers. The as-obtained catalyst Ni-P/NFM with 4.55 g/m^2 nanofibers exhibits the excellent performance for hydrogenation of nitrophenols to aminophenols at 20 °C with a rate constant of 18.04×10^{-3} s^{-1}, 26.84×10^{-3} s^{-1} and 19.40×10^{-3} s^{-1} for Ni-P loading content 50 wt.%, 25 wt.% and 14 wt.%, respectively, as well as a cyclic PNP conversion over 98% after 6 times. The high catalytic performance of the catalyst can be ascribed to the synergistic effect of 3D open-cell network configuration of the polymeric nanofibrous membrane, noncrystalline structure of nickel-based catalyst and phosphorus doping. Furthermore, present Ni-P-based catalyst is relatively cheap, stable and direct separable, facilitates achieving the cost-effective reduction of nitrophenols to aminophenols.

Acknowledgments

The authors were thankful to the financial support of National Natural Science Foundation of China (Nos. 51401149, 51273152 and 51473129), National Science-technology Support Program of China (No. 2015BAE01B01), Program for New Century Excellent Talents in University (No. 2013AA031802), Innovation Group Project of Science and Technology Department of Hubei province (No. 2015CFA028) and Excellent Young and Middle-aged Innovation Team Project of Education Department of Hubei province (No. T201408).

References

[1] Clean Water Act Priority Pollutant List. In: U.S.E.P. Agency (Ed.), CFR423, Appendix A, Code of Federal Regulations, 1982.
[2] Z. Jiang, J. Xie, D. Jiang, X. Wei, M. Chen, CrystEngComm 15 (2013) 560–569.
[3] M. Barreto-Rodrigues, F.T. Silva, T.C.B. Paiva, J. Hazard. Mater. 165 (2009) 1224–1228.
[4] Z. Jiang, J. Xie, D. Jiang, J. Jing, H. Qin, CrystEngComm 14 (2012) 4601–4611.
[5] Y. Lu, Y. Mei, M. Ballauff, M. Drechsler, J. Phys. Chem. B 110 (2006) 3930–3937.
[6] Y.-g. Wu, M. Wen, Q.-s. Wu, H. Fang, J. Phys. Chem. C 118 (2014) 6307–6318.
[7] D. Zhang, L. Chen, G. Ge, Catal. Commun. 66 (2015) 95–99.
[8] K. Hayakawa, T. Yoshimura, K. Esumi, Langmuir 19 (2003) 5517–5521.
[9] Caijin Huang, Jinli Hu, Wenjie Fan, Xin Wu, Xiaoqing Qiu, Chem. Eng. Sci. 131 (2015) 155–161.
[10] Y. Du, H. Chen, R. Chen, N. Xu, Appl. Cata. A: Gen. 277 (2004) 259–264.
[11] H. Lu, H. Yin, Y. Liu, T. Jiang, L. Yu, Catal. Commun. 10 (2008).
[12] G. Shi, L. Su, K. Jin, Catal. Commun. 59 (2015) 180–183.
[13] Y. Shi, Y. Xu, S. Zhuo, J. Zhang, B. Zhang, ACS Appl. Mater. Interfaces 7 (2015) 2376–2384.
[14] P. Bui, J.A. Cecilia, S.T. Oyama, A. Takagaki, A. Infantes-Molina, H. Zhao, D. Li, E. Rodríguez-Castellón, A.J. López, J. Catal. 294 (2012) 184–198.
[15] K. Li, R. Wang, J. Chem. Energy Fuels 25 (2011) 854–863.
[16] X. Song, Y. Ding, W. Chen, W. Dong, Y. Pei, J. Zang, L. Yang, Y. Lu, Chin. J. Catal. 33 (2012) 1938–1944.
[17] S. Tian, J. Chen, Fuel Process. Technol. 122 (2014) 120–128.
[18] P. Yang, Z. Jiang, P. Ying, C. Li, J. Catal. 253 (2008) 66–73.
[19] H. Wang, Z. Dong, C. Na, ACS Sustain. Chem. Eng. 1 (2013) 746–752.
[20] H. Liang, W. Zhang, Y. Ma, X. Cao, Q. Guan, W. Xu, S. Yu, ACS Nano 5 (2011) 8148–8161.
[21] T. Niu, J. Xu, W. Xiao, J. Huang, RSC Adv. 4 (2014) 4901–4904.
[22] S. Fazzini, D. Nanni, B. Ballarin, M.C. Cassani, M. Giorgetti, C. Maccato, A. Trapananti, G. Aquilanti, S.I. Ahmed, J. Phys. Chem. C 116 (2012) 25434–25443.
[23] K. Kuroda, T. Ishida, M. Haruta, J. Mol. Catal. A: Chem. 298 (2009) 7–11.
[24] Y. Zhu, J. Shen, K. Zhou, C. Chen, X. Yang, C. Li, J. Phys. Chem. C 115 (2010) 1614–1619.
[25] M.C. Demirel, M. Cetinkaya, A. Singh, W.J. Dressick, Adv. Mater. 19 (2007) 4495–4499.
[26] J. Macanas, L. Ouyang, M.L. Bruening, M. Muñoz, J.-C. Remigy, J.-F. Lahitte, Catal. Today 156 (2010) 181–186.
[27] D.M. Dotzauer, J. Dai, L. Sun, M.L. Bruening, Nano Lett. 6 (2006) 2268–2272.
[28] E.L. Warren, J.R. McKone, H.A. Atwater, H.B. Graya, N.S. Lewis, Energy Environ. Sci. 5 (2012) 9653.
[29] K. Eom, M. Kim, R. Kim, D. Nam, H. Kwon, J. Power Sources 195 (2010) 2830–2834.
[30] S. Zhang, S. Zhang, L. Song, X. Wu, S. Fang, Mater. Res. Bull. 53 (2014) 158–162.
[31] M. Li, X. Xue, Dong Wang, Y. Lu, Zhihong Wu, H. Zou, Desalination 329 (2013) 50–56.
[32] Y. Lu, Z. Wu, M. Li, Q. Liu, D. Wang, React. Funct. Polym. 82 (2014) 98–102.
[33] D. Wang, W. Xu, G. Sun, B.-s. Chiou, ACS Appl. Mater. Interfaces 3 (2011) 2838–2844.
[34] D. Wang, N. Liu, W. Xu, G. Sun, J. Phys. Chem. C 115 (2011) 6825–6932.
[35] Q. Liu, Z. Zhou, M. Xia, Y. Tao, K. Liu, D. Wang, RSC Adv. 4 (2013) 40788–40793.
[36] D. Wang, G. Sun, B.S. Chiou, Macromol. Mater. Eng. 292 (2007) 407–414.
[37] Z. Hou, J. Gao, J. Guo, D. Liang, H. Lou, X. Zheng, J. Catal. 250 (2007) 331–341.
[38] H. Pfeiffer, F. Tancret, T. Brousse, Mater. Chem. Phys. 92 (2005) 534–539.
[39] Y. Pan, Y. Liu, J. Zhao, K. Yang, J. Liang, D. Liu, W. Hu, D. Liu, Y. Liu, C. Liu, J. Mater. Chem. A 3 (2015) 1656–1665.
[40] J. Chen, S. Zhou, D. Ci, J. Zhang, R. Wang, J. Zhang, Indus. Eng. Chem. Res. 48 (2009) 3812–3819.
[41] G. Li, D. Zhang, J.C. Yu, Environ. Sci. Technol. 43 (2009) 7079–7085.
[42] A.M. Signori, K.d.O. Santos, R. Eising, B.L. Albuquerque, F.C. Giacomelli, J.B. Domingos, Langmuir 26 (2010) 17772–17779.
[43] S. Gu, S. Wunder, Y. Lu, M. Ballauff, J. Phys. Chem. C 118 (2014) 18618–18625.
[44] K.K. Soni, P.E.B.N. Rambabu, A.K. Dalai, J. Adjaye, Catal. Today 207 (2013) 119–126.
[45] L.T.H. Nguyen, S. Chen, N.K. Elumalai, M.P. Prabhakaran, Y. Zong, C. Vijila, S.I. Allakhverdiev, S. Ramakrishna, Macromol. Mater. Eng. 298 (2013) 822–867.
[46] D.S. Liu, J.N. Ashcraft, M.M. Mannarino, M.N. Silberstein, A.A. Argun, G.C. Rutledge, M.C. Boyce, P.T. Hammond, Adv. Funct. Mater. 23 (2013) 3087–3095.
[47] L.F. Dum, a.B.L. Li He, F.-M. Ailloux, J.-B. Lemoine, L. Velleman, F. She, M.C. Duke, J.D. Orbell, G. Erskine, P.D. Hodgson, S. Gray, a.L. Kong, J. Mater. Chem. A 1 (2013) 15185–15206.
[48] V.K. Bulasara, H. Thakuria, R. Uppaluri, M.K. Purkait, Desalination 268 (2011) 195–203.
[49] M. Li, G. Chen, Nanoscale 5 (2013) 11919–11927.
[50] Z. Ji, X. Shen, G. Zhu, H. Zhouc, A. Yuan, J. Mater. Chem. C 22 (2012) 3471–3477.
[51] X. Li, K. Wu, Y. Ye, X. Wei, Nanoscale 5 (2013) 3648–3653.
[52] J. Wei, Y. Ni, N. Xiang, Y. Zhang, X. Ma, CrystEngComm 16 (2014) 2113–2118.
[53] J. Xia, G. He, L. Zhang, X. Sun, X. Wang, Appl. Catal. B: Environ. 180 (2016) 408–415.
[54] C. Emin, J.-C. Remigy, J.-F. Lahitte, J. Membr. Sci. 455 (2014) 55–63.
[55] W. Wang, P. Liu, K. Wu, K. Zhang, L. Li, Z. Qiao, Y. Yang, N. J. Chem. 39 (2015) 813–816.
[56] S. Xie, M. Qiao, W. Zhou, G. Luo, H. He, K. Fan, T. Zhao, W. Yuan, J. Phys. Chem. B 109 (2005) 24361–24368.
[57] M. Mo, L. Han, J. Lv, Y. Zhu, L. Peng, X. Guo, W. Ding, Chem. Commun. 46 (2010) 2268–2270.
[58] Y. Zhu, F. Liu, W. Ding, X. Guo, Y. Chen, Angew. Chem. Int. Ed. 45 (2006) 7211–7214.
[59] A.R.J. Kucernak, V.N.N. Sundaram, J. Mater. Chem. A 2 (2014) 17435–17445.